Chapter 5

Effects of spherical aberration and defocusing on the near-field enhancement

This chapter presents a detailed investigation on a tightly focused linearly polarized beam under spherical aberration and its interaction with a nanoparticle. Impact of an aberrated focusing system on the scattering and localized surface enhancement is examined, and its role in the plasmonic response is highlighted. Effects of spherical aberration on the enhancement in near-field intensity is examined by separating its radial and tangential component. Enhancement factor obtained in an aberrated system in different dielectric media is compared with the results of an aberration free system. Unlike aberration free case, along with the radial component, a significant variation in the tangential component of the average intensity enhancement is also observed. To compensate the effect of spherical aberration, defocusing is used under the balancing condition.

5.1 Optical aberration

The term aberration means deviation from the ideal. Aberration can be analyzed by measuring distortion in the wavefront of the beam or by tracing individual light rays through an optical system [179]. Wave aberration in the optical system is described as a departure of the incident beam's wavefront from the Gaussian spherical wavefront. Here, we examine the wave aberration, and our special emphasis in this chapter is on the spherical aberration and defocusing. A Gaussian spherical wavefront represents that a system is aberration free, i.e. no wave aberration, and all the light rays converge to its center of curvature at the Gaussian point and a point is obtained, within the diffraction condition, as shown in Fig. 5.1 (a). On the other hand, aberrated system introduces a deviation in the wavefront with respect to the Gaussian spherical wavefront or Gaussian reference sphere as depicted in Fig. 5.1 (b).

The wave aberrations play a fundamental role in determining the performance of an optical system and hence their study is crucial in variety of scattering and microscopy related applications. Presence of an aberration in the optical system modifies the shape and size of the beam at the focus. The structure of the beam in the focal region gets altered for an aberrated system [180].

Aberration may exist in an optical system for a number of reasons. Due to geometrical misalignment of optical system, or imperfections in optical elements such as lenses and mirrors may lead to distortion of the wavefront [181-184]. On the other hand, a light ray experiencing mismatch in refractive index while propagating through an optical system also introduces deviation in size and shape of the focal spot, and introduces aberration in the system. Fig. 5.1 (c) shows a shifted focus due to aberration caused by propagation of a eam through an interface of two different materials.

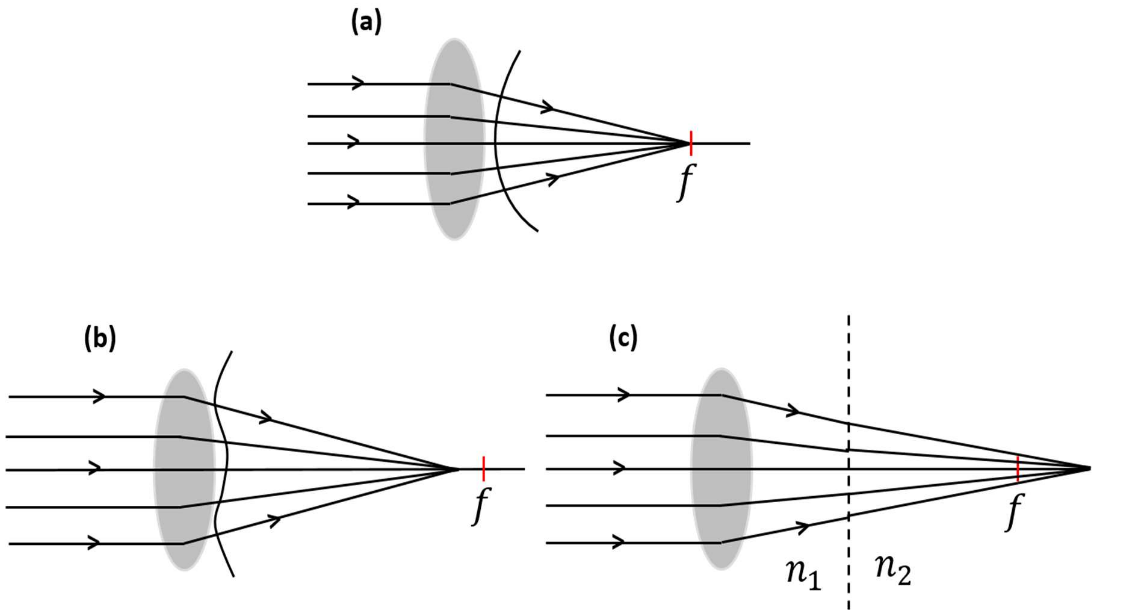

Fig. 5.1 (a) Rays converging to focus. Shifted focal point due to **(b)** aberrated wave front, **(c)** refractive index mis-match**.**

Based on the reason of distortion in the wave front of a wave, different kind of optical aberrations exist. Aberration existing due to dispersion of an optical element is said to be chromatic, and an optical lens do not focus light at a same focal point for different wavelengths of light. On the other hand, aberrations for a single wavelength due to the shape and geometry of the optical elements, is referred as monochromatic aberrations [179, 185]. Details analysis on nature of aberrations and their impacts on the optical testing and analysis is available in Ref. [186-198].

Aberrations mainly arise due to imperfections in the optical system or in the observation domain and few aberrated wavefronts are shown in Fig. 5.2, and the x-axis and y-axis have normalized units.

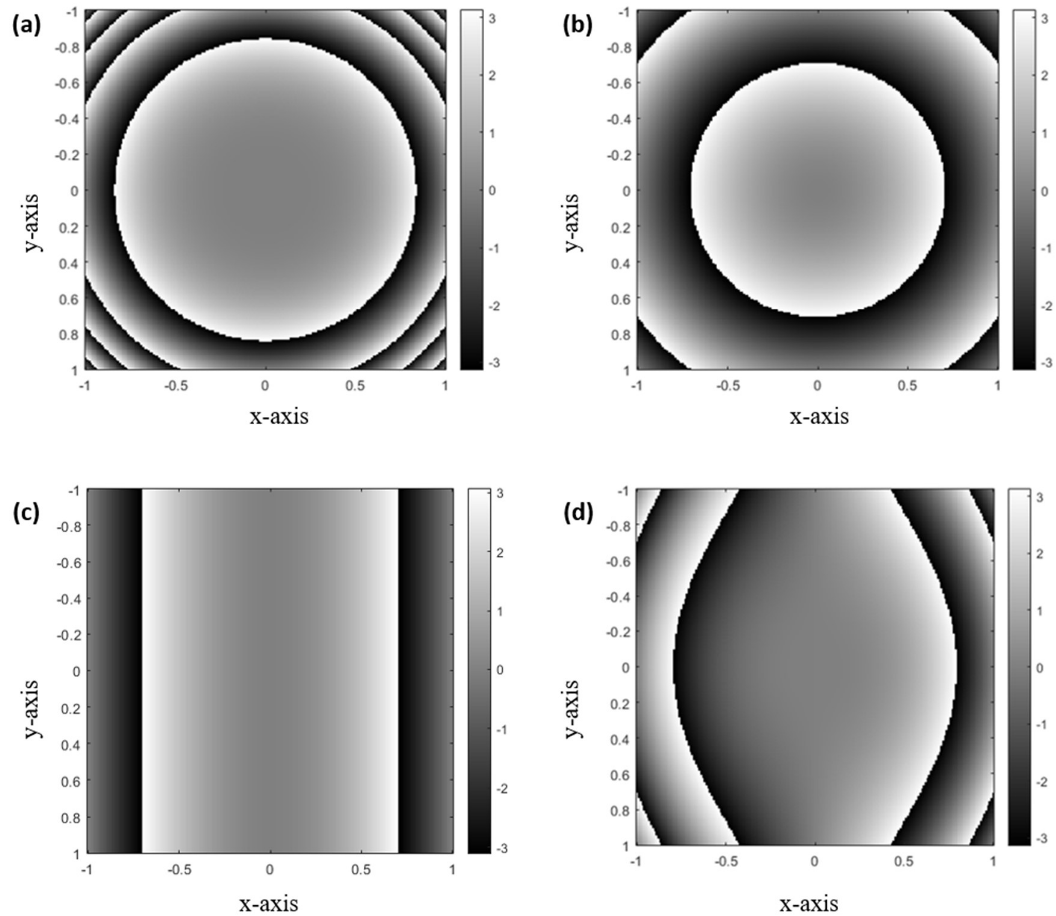

Fig. 5.2 Wavefront of (a) spherical aberration, (b) defocus, (c) astigmatism, and (d) coma aberration.

When a beam passes through a focusing lens, the marginal rays passing through the edges of the lens gets more deviated in comparison to the paraxial rays which passes through the center of the lens [100, 197]. Deviation in marginal rays causes non-collimation of marginal and paraxial rays at the desired ideal focus which becomes the reason of occurrence of spherical aberration in the optical system, which is a form of monochromatic axial wavefront aberration. Defocusing is a very common source of wavefront error which may arise due to a variety of reasons and one common source is deviation of the observation point or refractive index mismatch. Defocusing generally reduces the sharpness and contrast of focused beam.

In this chapter, we mainly emphasise on the presence of spherical aberration and defocusing in the system. The study focuses on investigating the interactions of a tightly focused beam with a nanoparticle in the presence of spherical aberration and defocusing. Due to a shift in focal point and distortion in the shape of focused beam, the interaction between a tightly focused beam and the scattering particle changes and this influences the scattering of light. Out of these primary aberrations, the spherical aberration and defocusing are commonly observed wavefront errors.

Therefore, a detailed study on the scattering of the tightly focused beams in the presence of spherical aberration and defocusing is taken in this chapter. Near field enhancement in the case of scattering of tightly focused beam with a nanoparticle is examined using the Mie scattering and multipole expansion. However, the examination of near-field intensity enhancement on the surface of nanoparticles by excitation from tightly focused beams seems to not exist despite of effects of the aberration observed on the focusing of the beam [198].

As discussed in **Chapter 3**, for a tightly focused beam, the electric $\boldsymbol{E}(\boldsymbol{r})$ and magnetic $\boldsymbol{H}(\boldsymbol{r})$ fields distribution at any point $P(x, y, z)$ in the focal region is given as [137]

$$\boldsymbol{E}(x, y, z) = -\frac{ik}{2\pi}\iint_{\Omega} \frac{\boldsymbol{a}(s_x, s_y)}{s_z} e^{ik[W(s_x, s_y)+s_x x+s_y y+s_z z]} ds_x ds_y, \tag{5.1}$$

$$\boldsymbol{H}(x, y, z) = -\frac{ik}{2\pi}\iint_{\Omega} \frac{\boldsymbol{b}(s_x, s_y)}{s_z} e^{ik[W(s_x, s_y)+s_x x+s_y y+s_z z]} ds_x ds_y \tag{5.2}$$

For an aberrated optical system $\mathrm{W}(s_x, s_y)$ becomes non-zero. The components of a unit vector $\boldsymbol{s}$, and the position vector $\vec{r}_p$ in the spherical coordinate system is expressed as

$s_x = sin\theta\ cos\phi$, $s_y = sin\theta\ sin\phi$, and $s_z = cos\theta$,

$x = r_P\ sin\theta_P\ cos\phi_P$, $y = r_P\ sin\theta_P\ sin\phi_P$, and $z = r_P\ cos\theta_P$.

Based on Richard and Wolf's formalism, the complex electric field for a tightly focused linearly polarized beam along x-axis, in the presence of an optical aberration is given as

$$\boldsymbol{E}(\vec{r}) = -\frac{ie^{ikf}E_0}{\lambda}\int_0^{2\pi}\int_0^{\alpha} e^{ikW(\theta,\phi)}A(\theta)\begin{bmatrix} cos\theta\, cos^2\phi + sin^2\phi \\ cos\theta\, cos\phi\, sin\phi - sin\phi\, cos\phi \\ -cos\phi\, sin\theta \end{bmatrix} \times \exp\left(i\vec{k}.\vec{r}\,\right) sin\theta d\theta d\phi \qquad (5.3)$$

where $W(\theta,\phi)$ represents the wave aberration function in the optical system, which is expressed using Zernike polynomials. Other variables have been defined in previous chapters.

5.2 Wave aberrations and Zernike polynomial

To describe the presence of primary aberration function of an optical system, Zernike polynomials have been extensively used. Most of optical systems have circular or annular apertures, and Zernike polynomials are useful in wavefront analysis [185, 199-203]. These polynomials are defined as the complete set of continuous functions over a unit disk, and hence, the aberration of such optical systems in a power series expansion or in a complete set of orthogonal polynomials. To examine the effects of primary aberrations, the aberration in circular symmetric optical system is interpreted by Zernike polynomial. Generally, spherical aberration and defocus are dominant in the phase function, and these can be expanded into finite terms of Zernike polynomial as

$$W(\theta) = A_s\left(\frac{sin\theta}{sin\alpha}\right)^4 + A_d\left(\frac{sin\theta}{sin\alpha}\right)^2 \qquad (5.4)$$

where A_s and A_d are the coefficients of Zernike polynomial associated with spherical aberration and defocusing in wavelength units [185]. It has been observed that an appropriate value of defocusing aberration can be used to reduce the effect of spherical aberration. Effect of spherical aberration on the focal spot can be reduced by using a balancing condition, i.e. $A_d = -A_s$.

Due to the spherical aberration and defocusing in the optical system, the electric field components (E_x, E_y, E_z) near the focus are written as [137]

$$E_x(v, u, \phi_P) = K[I_0 + I_2\, cos(2\phi_P)] \tag{5.5}$$

$$E_y(v, u, \phi_P) = KI_2\, sin(2\phi_P) \tag{5.6}$$

$$E_z(v, u, \phi_P) = -2iKI_1 \cos(\phi_P) \tag{5.7}$$

where $K = -\left(\frac{ik}{2}\right) f exp(ikf) E_0$,

$$I_0(v, u) = \int_0^\alpha A(\theta)\, exp(ikW(\theta))\, sin(\theta)\, [1 + \cos(\theta)]\, J_0\left[\frac{v}{sin\,\alpha} sin\,\theta\right]$$

$$\times\, exp\left[i \frac{u}{sin^2\alpha} cos(\theta)\right] d\theta, \tag{5.8}$$

$$I_1(v, u) = \int_0^\alpha A(\theta) \exp\big(ikW(\theta)\big)\, sin^2(\theta)\, J_1\left[\frac{v}{sin\,\alpha} sin\,\theta\right]$$

$$\times\, exp\left[i \frac{u}{sin^2\alpha} cos(\theta)\right] d\theta, \tag{5.9}$$

$$I_2(v, u) = \int_0^\alpha A(\theta) \exp(ikW(\theta))\, sin(\theta)\, [1 - \cos(\theta)]\, J_2\left[\frac{v}{sin\,\alpha} sin\,\theta\right]$$

$$\times\, exp\left[i \frac{u}{sin^2\alpha} cos(\theta)\right] d\theta. \tag{5.10}$$

Here, $J_n\left[\frac{v}{sin\,\alpha} sin\,\theta\right]$ is the Bessel functions of the first kind with $v = kr_p sin\,\theta_P\, sin\,\alpha = k\sqrt{x^2 + y^2}\, sin\,\alpha$, and $u = kr_p cos\,\theta_P\, sin^2\alpha$.

We evaluated the electric field components (E_x, E_y, E_z) at the focus of a tightly focused linearly polarized beams with spherical aberration coefficients $A_s = 0.5\lambda$, and $A_s = 1.0\lambda$ in Fig. 5.2

(a), and Fig. 5.2 (b) respectively for an incident wavelength $\lambda = 645\ nm$. Here, we simulated these results for a convergence angle $\alpha = 60°$.

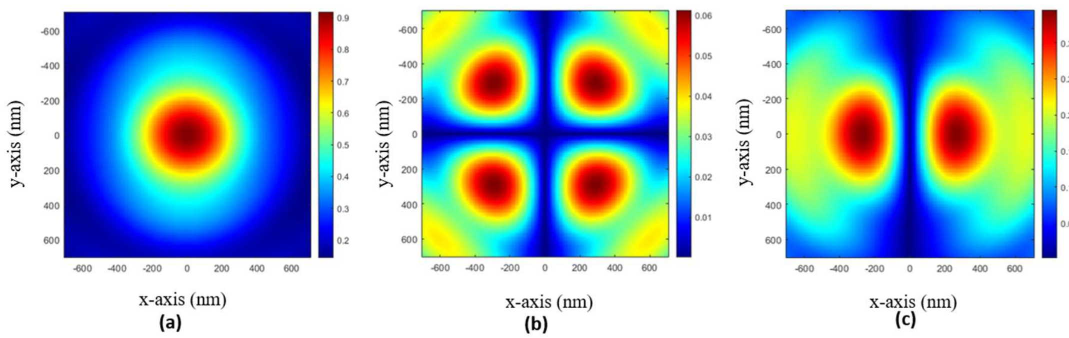

Fig. 5.3 Electric field components of a tightly focused linearly polarized beam at the focal plane under spherical aberration ($\boldsymbol{A_s = 0.5\lambda}$) (a) $\boldsymbol{E_x(x, y)}$, (b) $\boldsymbol{E_y(x, y)}$, and (c) $\boldsymbol{E_z(x, y)}$. The results are normalized with the maximum value of the total absolute value of the electric field**.**

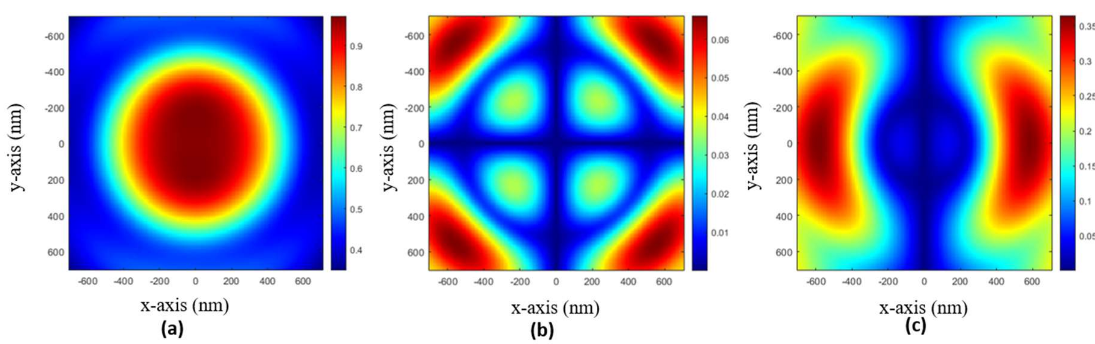

Fig. 5.4 Electric field components of a tightly focused linearly polarized beam at the focal plane under spherical aberration ($\boldsymbol{A_s = 1.0\lambda}$) (a) $\boldsymbol{E_x(x, y)}$, (b) $\boldsymbol{E_y(x, y)}$, and (c) $\boldsymbol{E_z(x, y)}$. The results are normalized with the maximum value of the total absolute value of the electric field.

Effect of spherical aberration is apparent in comparison to electrical field components of an aberration free tightly focused beam (Fig. 3.3, **Chapter 3**).

5.3 Mie Scattering for a tightly focused linearly polarized beam under spherical aberration and defocusing

The Richard and Wolf's formalism combined with the Mie scattering theory explains the scattering of the tightly focussed beam with a nanoparticle in the presence of optical aberration in the system. Fig. 5.5 shows the scattering of a spherically aberrated tightly focused linearly polarized beam by a spherical nanoparticle. S is wavefront curvature in presence of spherical aberration, which is deviated from the Gaussian reference sphere as represented by the dotted line.

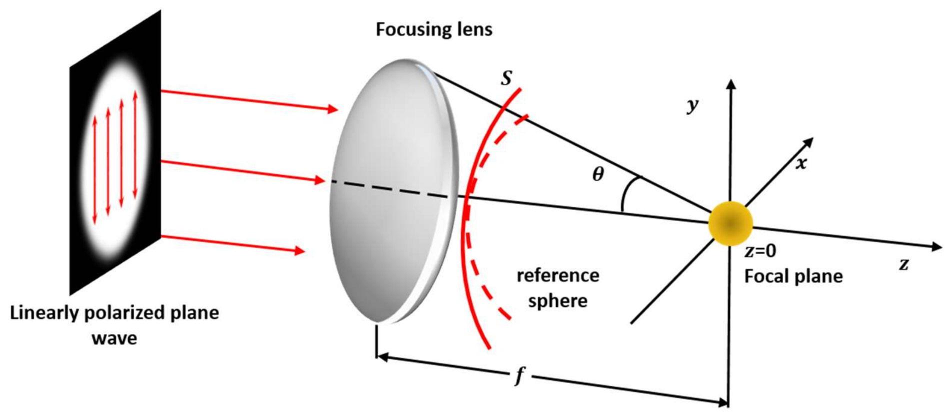

Fig. 5.5 Scattering of a spherically aberrated tightly focused linearly polarized beam by a spherical nanoparticle.

Considering the notation of multipoles, and vector spherical harmonics, the incident and the scattered electric fields for a tightly focused linearly polarized beam under spherical aberration are expressed as

$$\boldsymbol{E}_i = \sum_{n=1}^{\infty} A_n (\boldsymbol{N}_{e1n}^{(1)} - i\boldsymbol{M}_{o1n}^{(1)}), \tag{5.11}$$

$$\boldsymbol{E}_s = \sum_{n=1}^{\infty} A_n (-a_n \boldsymbol{N}_{e1n}^{(3)} + i b_n \boldsymbol{M}_{o1n}^{(3)}), \tag{5.12}$$

where $\boldsymbol{M}_{o1n}$, $\boldsymbol{N}_{e1n}$ are the vector spherical harmonics which are the function of the associated Legendre polynomial. n are the integers representing dipole, quadrupole, and higher multipole orders. Superscripts $^{(1)}$ and $^{(3)}$ denote the spherical Bessel function $(j_n(\rho))$ and the spherical Hankel function of the first kind $(h_n^{(1)}(\rho))$ respectively.

In presence of spherical aberration, the expansion coefficient A_n for a tightly focused linearly polarized beam is expressed as

$$A_n = (-i)^n E_0 kf \frac{2n+1}{2n^2(n+1)^2} \int_0^{\alpha} e^{ikW(\theta)} A(\theta) \left[\frac{P_n^1(cos\theta)}{sin\theta} + \frac{dP_n^1(cos\theta)}{d\theta}\right] sin\theta d\theta, \quad (5.13)$$

where $P_n^1(cos\theta)$ is the associated Legendre polynomial. The scattering coefficients a_n, and b_n are given as

$$a_n = \frac{m_0\psi_n(m_0x)\psi_n'(x) - \psi_n(x)\psi_n'(m_0x)}{m_0\psi_n(m_0x)\chi_n'(x) - \chi_n(x)\psi_n'(m_0x)}, \quad (5.14)$$

$$b_n = \frac{\psi_n(m_0x)\psi_n'(x) - m_0\psi_n(x)\psi_n'(m_0x)}{\psi_n(m_0x)\chi_n'(x) - m_0\chi_n(x)\psi_n'(m_0x)}, \quad (5.15)$$

where $\psi_n(\rho) = \rho j_n(\rho)$ and $\chi_n(\rho) = \rho h_n^{(1)}(\rho)$ are the Riccati-Bessel functions, $\psi_n'(\rho)$ and $\chi_n'(\rho)$ are the respective first order derivatives. $x = ka$ is the size parameter, a is the radius of the metallic nanoparticle. $m_0 = \frac{k_1}{k}$ is the relative refractive index with the respective surrounding medium. $k = \frac{2\pi}{\lambda}\, \tilde{n}_{medium}$, is the wave vector in a surrounding medium and $k_1 = \frac{2\pi}{\lambda}\, \tilde{n}_{particle}$, is the wave vector inside the nanoparticle [65].

5.4 Near-field intensity enhancement for an aberrated system

The average intensity enhancement in the near-field, representing the enhancement factor, is given by the total field intensity averaged over the nanoparticle's surface and normalized by the intensity at the nanoparticle's center [72, 80]. The average intensity enhancement in the near-field of a nanoparticle holds interests in various fields because of unique plasmonic properties of the nanoparticles. When a tightly focused linearly polarized beam under spherical aberration is scattered from a nanoparticle, the average radial (K_r) and tangential intensity (K_t) enhancements in the near-field are expressed as

$$K_r = \frac{9}{16(ka)^4} \sum_n \frac{|A_n|^2}{|A_1|^2} \frac{2n^3(n+1)^3}{2n+1} [|a_n|^2 |\chi_n|^2 + |\psi_n|^2 - 2\, Re\{a_n \chi_n\} \psi_n], \qquad (5.16)$$

$$K_t = \frac{9}{16(ka)^4} \sum_n \frac{|A_n|^2}{|A_1|^2} \frac{2n^2(n+1)^2}{2n+1} [|a_n|^2 \left|\chi_n^{'}\right|^2 + |b_n|^2 |\chi_n|^2 + |\psi_n|^2 + \left|\psi_n^{'}\right|^2$$
$$-2\, Re\{a_n \chi_n^{'}\} \psi_n^{'} - 2\, Re\{b_n \chi_n\} \psi_n]. \qquad (5.17)$$

The expansion coefficient, and scattering coefficients under spherical aberration is substituted from Eq. (5.13), and Eqs. (5.14-5.15) respectively.

5.5 Results and Discussion

Apart from several limitations mentioned earlier about modelling of a tightly focused beam in COMSOL, another limitation is introducing aberration in the light source. Therefore, we developed our own Mie scattering algorithm on the MATLAB platform, for examining the effects of spherical aberration and defocusing on the interaction of a tightly focused linearly polarized beam with a nanoparticle. A detailed study is made to examine the near field intensity enhancement on the surface of a monometallic nanoparticle using MATLAB platform.

An Au and Ag spherical nanoparticle of radius $a = 50\ nm$, is considered for this investigation. The average radial and tangential intensity enhancement for a tightly focused aberrated beam having maximum convergence angle $\alpha = 60°$, is obtained, for two different dielectric media air and BK7 (glass). The refractive index of the dispersive medium BK7 (glass) is considered from Eq. 2.17 (**Chapter 2**). We have considered $n = 7$ multipole order in the evaluation of intensity enhancement. The optical constants of Au, and Ag are taken from Johnson and Christy [132].

The coefficient A_s represents the strength of spherical aberration in the system, and $A_d = 0$ is considered. In Fig. 5.6 to Fig. 5.9, the values considered for spherical aberration coefficient (A_s) are: 0.5λ, 1.0λ, 1.5λ, 2.0λ, 2.5λ, 3.0λ, 3.5λ, 4.0λ. Since, a different pattern for half integral A_s $(0.5\lambda, 1.5\lambda, 2.5\lambda, 3.5\lambda)$, and integral A_s $(1.0\lambda, 2.0\lambda, 3.0\lambda, 4.0\lambda)$ are observed. The examination of intensity enhancement in near-field for a spherically aberrated tightly focused beam is done separately for half-integral and integral coefficients of spherical aberration.

Fig. 5.6 shows the average intensity enhancement for an Au particle illuminated by a tightly focused linearly polarized beam. For an aberration free optical system, i.e. $A_s = 0.0\lambda$, the maximum radial enhancement is 10.65 at a wavelength 546 nm, and the maximum tangential enhancement is 1.082 observed at wavelength 521 nm. Fig. 5.6 (a), and Fig. 5.6 (b) represents the average radial and tangential intensity enhancement respectively, for the half-integral A_s $(0.5\lambda, 1.5\lambda, 2.5\lambda, 3.5\lambda)$, for which the curves are overlapping. On the other hand, the average radial and tangential intensity enhancement factor for integral A_s $(1.0\lambda, 2.0\lambda, 3.0\lambda, 4.0\lambda)$ are shown in Fig. 5.6 (c), and Fig. 5.6 (d) respectively. A significant variation in intensity enhancement, for different value of A_s is observed. The inset plots highlight the increment in the enhancement factor. The maximum radial and tangential enhancement factors of value 11.09, and 1.124 respectively are observed for $A_s = 1.0\lambda$ as shown in Figs. 5.6 (c), and (d).

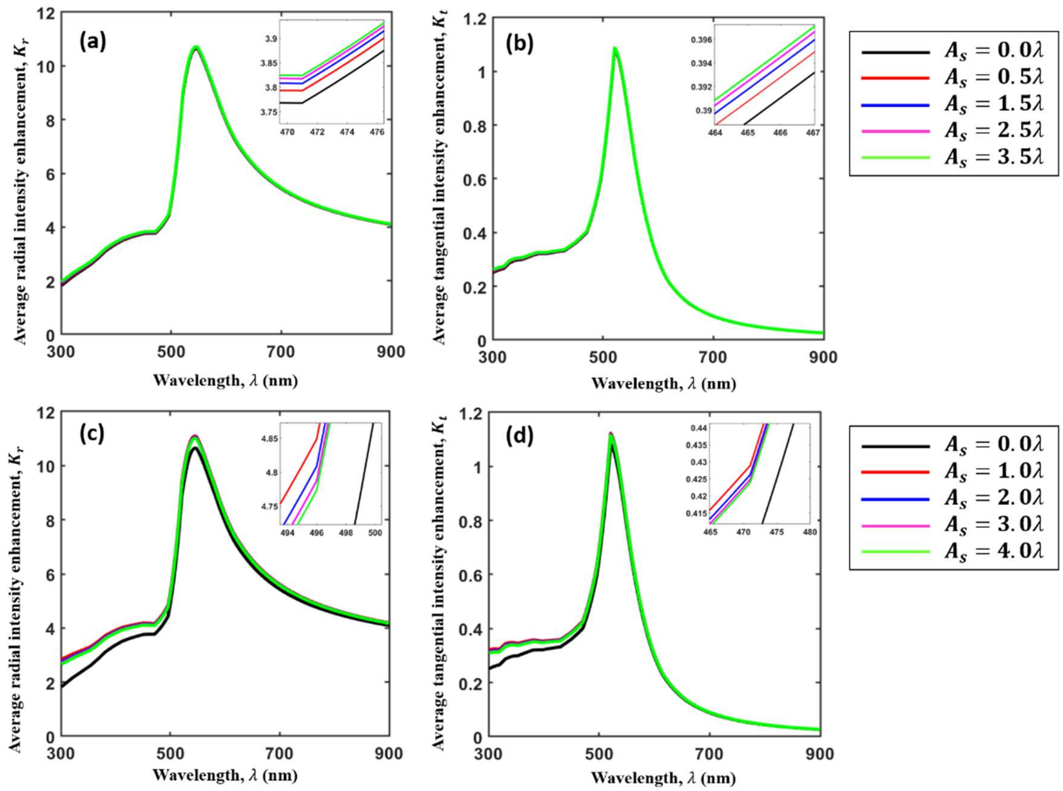

Fig. 5.6 Average radial and tangential intensity enhancement for a spherically aberrated tightly focused linearly polarized beam having wavelength ranging from 300 nm to 900 nm scattering by an Au nanoparticle in air, respectively for (a), (b) half-integral $\boldsymbol{A_s = 0.5\lambda, 1.5\lambda, 2.5\lambda, 3.5\lambda}$; and (c), (d) integral $\boldsymbol{A_s = 1.0\lambda, 2.0\lambda, 3.0\lambda, 4.0\lambda}$.

Using the data from Fig. 5.6 (a-d), the maximum intensity enhancement for different value of A_s are tabulated in Table 5.1. Table 1 shows the variation in value of average radial and tangential intensity enhancement for different values of A_s.

Table 5.1: Intensity enhancement observed for an Au nanoparticle in air

Aberration free case: $A_s = 0.0\lambda$	Average radial intensity enhancement		10.65	
	Average tangential intensity enhancement		1.082	
Half-integral spherical aberration coefficients	$A_s = 0.5\lambda$	$A_s = 1.5\lambda$	$A_s = 2.5\lambda$	$A_s = 3.5\lambda$
Average radial intensity enhancement	10.67	10.69	10.70	10.71
Average tangential intensity enhancement	1.084	1.086	1.087	1.088
Integral spherical aberration coefficients	$A_s = 1.0\lambda$	$A_s = 2.0\lambda$	$A_s = 3.0\lambda$	$A_s = 4.0\lambda$
Average radial intensity enhancement	11.09	11.05	11.02	11.01
Average tangential intensity enhancement	1.124	1.120	1.117	1.116

The near-field intensity enhancement is analyzed for scattering a tightly focused aberrated beam from an Au nanoparticle in a BK7 (glass) medium and the results are shown in Fig. 5.7 for different A_s. For an aberration-free system i.e., $A_s = 0.0$, the average radial intensity enhancement is 16.21 at a wavelength 643 nm, whereas the average tangential intensity enhancement is 2.301 at a wavelength 602 nm. The average radial and tangential intensity enhancement for the half-integral A_s $(0.5\lambda, 1.5\lambda, 2.5\lambda, 3.5\lambda)$ are shown in Fig. 5.7 (a), and Fig. 5.7 (b) respectively. For integral A_s $(1.0\lambda, 2.0\lambda, 3.0\lambda, 4.0\lambda)$, Fig. 5.7 (c), and Fig. 5.7 (d) represent the average radial and tangential intensity enhancement respectively. A significant enhancement in radial and tangential intensities are observed for integral coefficient. The highest value of enhancement in radial intensity is 17.18 for $A_s = 1.0\lambda$ spherical aberration at a wavelength 643 nm. On the other hand, the maximum average tangential intensity enhancement is 2.492 at 593 nm wavelength. LSPR peak in the average tangential intensity enhancement is also slightly shifted for focusing system with integral A_s as shown in Fig. 5.7 (d).

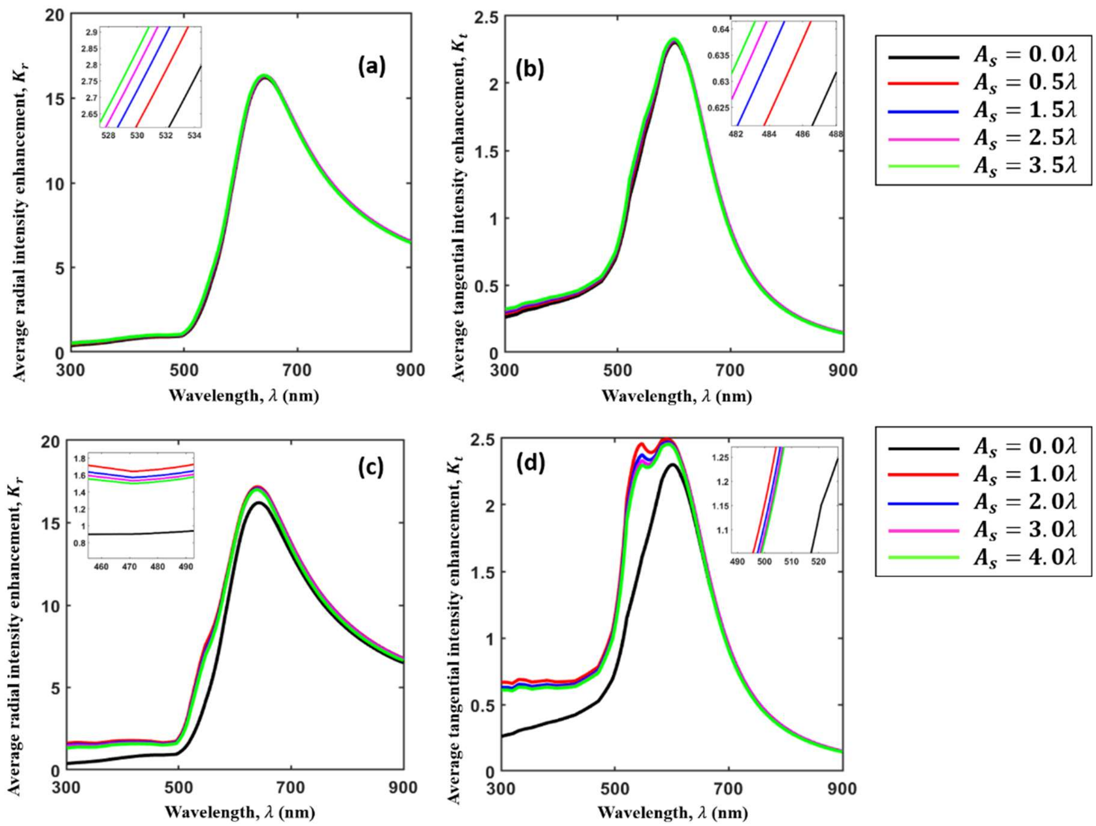

Fig. 5.7 Average radial and tangential intensity enhancement for a spherically aberrated tightly focused linearly polarized beam with wavelength range 300 nm to 900 nm and scattering by an Au nanoparticle in BK7 (glass) for (a), (b) half-integral $A_s = 0.5\lambda, 1.5\lambda, 2.5\lambda, 3.5\lambda$; and (c), (d) integral $A_s = 1.0\lambda, 2.0\lambda, 3.0\lambda, 4.0\lambda$.

Table 5.2 shows the maximum intensity enhancement for different value of A_s in the system, and the data are extracted from Fig. 5.7 (a-d). Change in the intensity enhancement is higher for A_s with integral value in comparison to the results obtained for A_s with half-integral as presented in Table 5.2.

Table 5.2: Intensity enhancement for an Au nanoparticle in glass

Aberration free case: $A_s = 0.0\lambda$	Average radial intensity enhancement		16.21	
	Average tangential intensity enhancement		2.301	
Half-integral spherical aberration coefficients	$A_s = 0.5\lambda$	$A_s = 1.5\lambda$	$A_s = 2.5\lambda$	$A_s = 3.5\lambda$
Average radial intensity enhancement	16.27	16.31	16.33	16.35
Average tangential intensity enhancement	2.312	2.319	2.323	2.328
Integral spherical aberration coefficients	$A_s = 1.0\lambda$	$A_s = 2.0\lambda$	$A_s = 3.0\lambda$	$A_s = 4.0\lambda$
Average radial intensity enhancement	17.18	17.09	17.03	17.00
Average tangential intensity enhancement	2.492	2.471	2.460	2.454

The scattering of a tightly focused beam under spherical aberration from an Ag nanoparticle in air is investigated and results are presented in Fig. 5.8 for different spherical aberration coefficients. Fig. 5.8 (a), and Fig. 5.8 (b) shows the average radial and tangential intensity enhancement factors respectively, for A_s with half-integral values $(0.5\lambda, 1.5\lambda, 2.5\lambda, 3.5\lambda)$. On the other hand, the average intensity enhancement factors respectively, for integral A_s

$(1.0\lambda, 2.0\lambda, 3.0\lambda, 4.0\lambda)$ are presented in Fig. 5.8 (c), and Fig. 5.8 (d). The average radial intensity enhancement for an aberration free system is 18.10 at a wavelength 407 nm. On the other hand, the average tangential intensity enhancement for an aberration free system reaches to 3.447 at 353 nm as shown in Fig. 5.8.

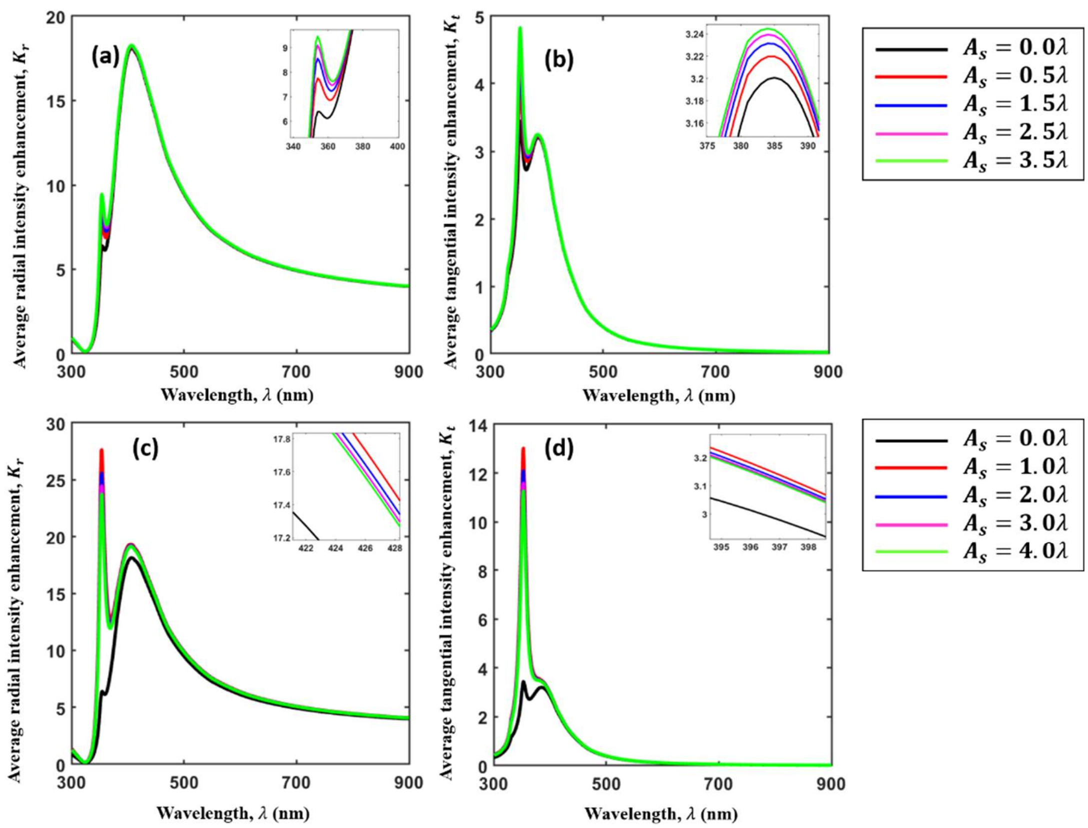

Fig. 5.8 Average radial and tangential intensity enhancement for a spherically aberrated tightly focused linearly polarized beam within wavelength range 300 nm to 900 nm and scattering by an Ag nanoparticle in air for (a), (b) half-integral $\boldsymbol{A_s = 0.5\lambda, 1.5\lambda, 2.5\lambda, 3.5\lambda}$; and (c), (d) integral $\boldsymbol{A_s = 1.0\lambda, 2.0\lambda, 3.0\lambda, 4.0\lambda}$.

Since Ag exhibits resonance of higher multipole order than dipolar order, therefore more than one LSPR peaks are observed. In Fig. 5.8 (b) it can be seen that in presence of spherical aberration the maximum intensity enhancement factor is observed due to second order LSPR peak for a half-integral A_s. Similarly, for integral A_s, the maximum enhancement factor is observed due to a second order LSPR peak as shown in Figs. 5.8 (c), and (d). Fig. 5.8 (c) highlights that the second order LSPR peak with maximum average radial intensity enhancement occurs at wavelength 354 nm. The highest radial and tangential intensity enhancement factors become 27.66, and 13.03, respectively, for a tightly focused beam with $A_s = 1.0\lambda$. Table 5.3 presents the maximum values of average radial and tangential enhancement factors for different values of A_s, and the data representing the maximum intensities are manually extracted from Figs. 5.8 (a-d).

Table 5.3: Intensity enhancement for an Ag nanoparticle in air

Aberration free case: $A_s = 0.0\lambda$	Average radial intensity enhancement	18.10		
	Average tangential intensity enhancement	3.447		
Half-integral spherical aberration coefficients	$A_s = 0.5\lambda$	$A_s = 1.5\lambda$	$A_s = 2.5\lambda$	$A_s = 3.5\lambda$
Average radial intensity enhancement	18.17	18.22	18.25	18.27
Average tangential intensity enhancement	4.063	4.426	4.667	4.831
Integral spherical aberration coefficients	$A_s = 1.0\lambda$	$A_s = 2.0\lambda$	$A_s = 3.0\lambda$	$A_s = 4.0\lambda$
Average radial intensity enhancement	27.66	25.58	24.47	23.75
Average tangential intensity enhancement	13.03	12.09	11.59	11.27

The near-field intensity enhancement is investigated in Fig. 5.9 for an Ag nanoparticle of 50 nm radius in BK7 (glass) illuminated by a tightly focused linearly polarized beam under spherical aberration. Three LSPR peaks are observed for an Ag nanoparticle in glass medium and this shows the involvement of higher multipole orders. For an aberration free system as shown in Fig. 5.9, a maximum average radial intensity enhancement of 12.85 is observed at 588 nm wavelength, and another peak representing higher modes shows the enhancement factor of 12.27 at wavelength 419 nm. On the other hand, the average tangential intensity enhancement is of the order 4.873 at wavelength 417 nm.

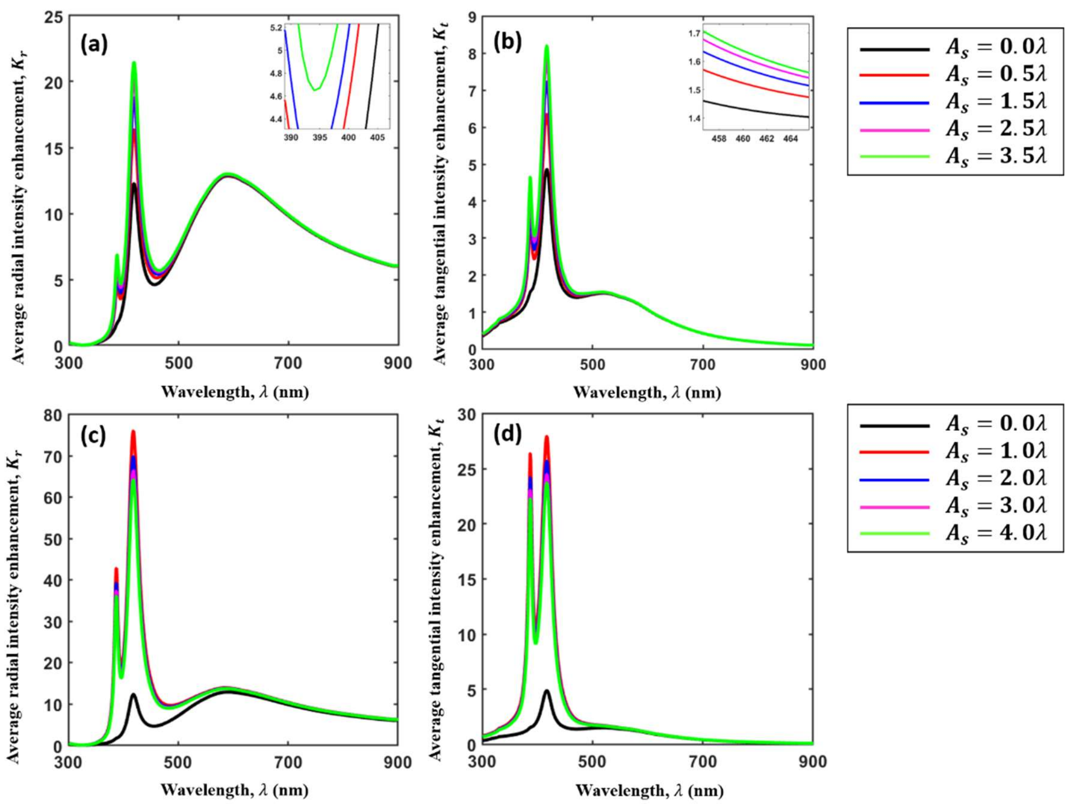

Fig. 5.9 Average radial and tangential intensity enhancement for a spherically aberrated tightly focused linearly polarized beam having wavelength range 300 nm to 900 nm and scattering by an Ag nanoparticle in BK7 (glass) for (a), (b) half-integral $\boldsymbol{A_s} = \mathbf{0.5\lambda, 1.5\lambda, 2.5\lambda, 3.5\lambda}$; and (c), (d) integral $\boldsymbol{A_s} = \mathbf{1.0\lambda, 2.0\lambda, 3.0\lambda, 4.0\lambda}$.

Fig. 5.9 (a), and Fig. 5.9 (b) represents the average radial and tangential intensity enhancement factors respectively, due to A_s with half-integral values $(0.5\lambda, 1.5\lambda, 2.5\lambda, 3.5\lambda)$. On the other hand, the average radial and tangential intensity enhancement factors for A_s with the integral values $(1.0\lambda, 2.0\lambda, 3.0\lambda, 4.0\lambda)$ are shown in Fig. 5.9 (c), and Fig. 5.9 (d), respectively. It is observed that in presence of spherical aberration, a maximum intensity enhancement factor is observed due to a second order LSPR peak as shown in Figs. 5.9 (a-d). Table 5.4 presents the data for maximum value of enhancement factor for radial and tangential component of average intensity, which is obtained from Figs. 5 (a-d) for different strengths of the A_s. For an aberrated system having spherical aberration of $A_s = 1.0\lambda$, it is observed that the maximum radial and tangential intensity enhancement factors reach to values 75.93 and 27.94 respectively.

Table 5.4: Intensity enhancement for an Ag nanoparticle in glass

Aberration free case: $A_s = 0.0\lambda$	Average radial intensity enhancement		12.85	
	Average tangential intensity enhancement		4.873	
Half-integral spherical aberration coefficients	$A_s = 0.5\lambda$	$A_s = 1.5\lambda$	$A_s = 2.5\lambda$	$A_s = 3.5\lambda$
Average radial intensity enhancement	16.35	18.76	20.36	21.45
Average tangential intensity enhancement	6.353	7.229	7.811	8.206
Integral spherical aberration coefficients	$A_s = 1.0\lambda$	$A_s = 2.0\lambda$	$A_s = 3.0\lambda$	$A_s = 4.0\lambda$
Average radial intensity enhancement	75.93	69.72	66.40	64.23
Average tangential intensity enhancement	27.94	25.69	24.48	23.70

It is observed that the enhancement factor is high in BK7 (glass) in comparison to the air. The intensity enhancement depends on the refractive index, electric permittivity of the surrounding medium, and the nanoparticle. These two different materials have refractive indices ($n_{air} = 1$, and for dispersive materials $n_{glass} = 1.55 \sim 1.50$ for wavelength ranging from 300 nm to 900 nm). Since refractive index of BK7 is greater than air, so the intensity enhancement is high for BK7 in comparison to air.

The average radial and tangential intensity enhancement increases in the presence of spherical aberration as shown in Figs. 5.6 to 5.9. With increase in value of A_s, an increase in the value of the LSPR peak exhibiting maximum intensity amplification is seen. Usually, the radial component plays a major role in the near field but presence of a spherical aberration in the system alters this condition with increased strength of the tangential component as well. Hence, an increase in both the average radial and tangential intensity enhancements is observed.

The average radial and tangential intensity enhancement increases with increasing the value of A_s with strengths in order of half-integral i.e. $A_s = 0.5\lambda$ to $A_s = 3.5\lambda$ as shown in Tables 5.1 to 5.4. On the contrary, a maximum enhancement factor is observed for $A_s = 1.0\lambda$, and the enhancement factor decreases with further increase in the integral strength of the spherical aberration i.e. $A_s = 1.0\lambda$ to $A_s = 4.0\lambda$ as shown in Tables 5.1 to 5.4.

The data taken from Table 5.1 to 5.4 is presented in Fig. 5.10 to explain the observed pattern of average radial and tangential intensity enhancement for different values of A_s.

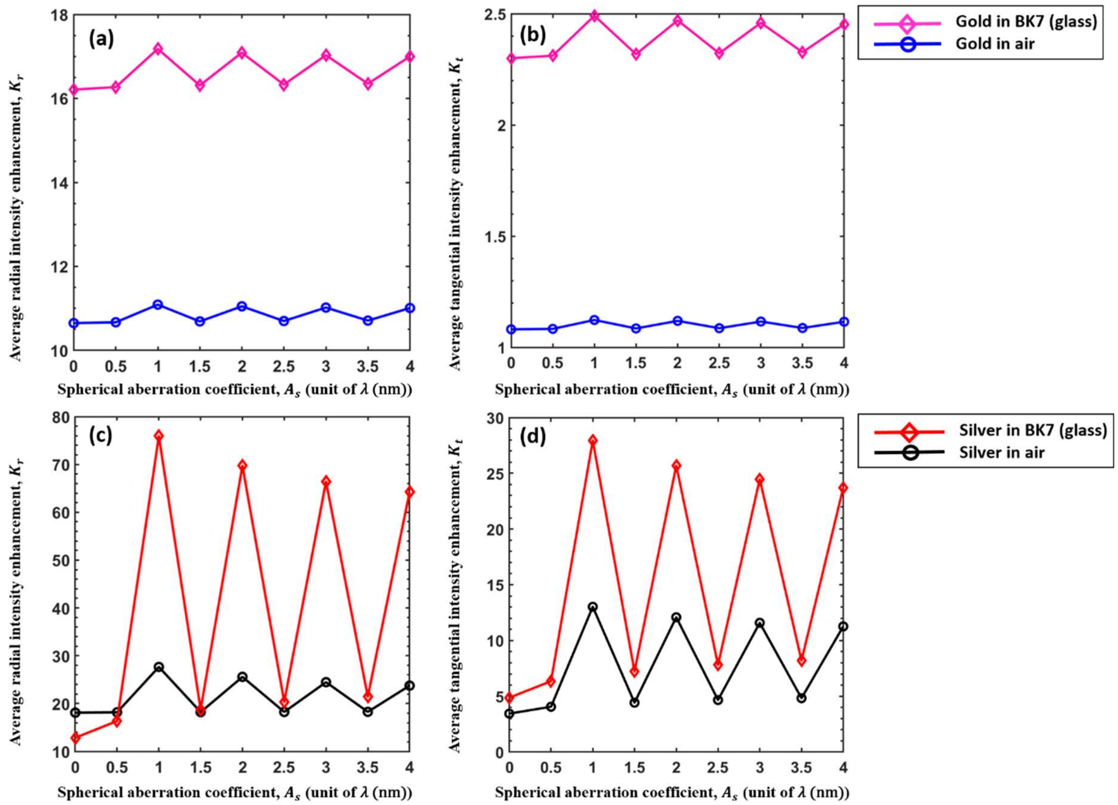

Fig. 5.10 Variation in average radial and tangential intensity enhancement with $\boldsymbol{A_s}$ respectively, for an (a), (b) Au nanoparticle and (c), (d) Ag nanoparticle in two different media air, BK7 (glass).

Fig. 5.10 shows how the intensity enhancement varies for a half-integral and integral A_s. Figs. 5.10 (a), and (b) shows the average radial and tangential intensity enhancement for different values of A_s in case of an Au nanoparticle. For an Ag nanoparticle, the variation of average radial and tangential intensity enhancement in air, and BK7 are presented in Figs. 5.10 (c), (d). Though the pattern of intensity enhancement is similar for an Au and Ag nanoparticle with increasing value of A_s, but it is clearly visible that an Ag nanoparticle shows a significant enhancement in both the media in comparison to an Au nanoparticle.

It is also observed that a single LSPR peaks is observed for an Au nanoparticle which arises mainly due to the contribution of a dipole order, whereas multiple LSPR peaks are observed for an Ag nanoparticle showing involvement of higher multipole orders. Figs. 5.6 to 5.9

highlight that an Ag nanoparticle shows a better intensity enhancement in all conditions in comparison to an Au nanoparticle. Ag nanoparticle shows a high scattering efficiency and low absorption efficiency, which leads to the high intensity enhancement. On the other hand, Au nanoparticle shows a low scattering efficiency, and hence lesser intensity enhancement in contrast to Ag nanoparticle.

It is noticed from Figs. 5.6 to 5.9, and Table 5.1 to 5.4, that under spherical aberration the intensity enhancement due to an integral A_s $(1.0\lambda, 2.0\lambda, 3.0\lambda, 4.0\lambda)$ is greater than that due to a half-integral A_s $(0.5\lambda, 1.5\lambda, 2.5\lambda, 3.5\lambda)$. This difference in behavior of coefficients of spherical aberration is accounted mainly due to the multipole order or modes contribution for individual case. Due to this reason a different pattern in variation of intensity enhancement is observed for integral, and half-integral A_s values. Fig. 5.11 shows the involvement of modes according to different values of A_s, which clearly gives the idea behind greater enhancement factor for integral coefficients in comparison to half-integral coefficients.

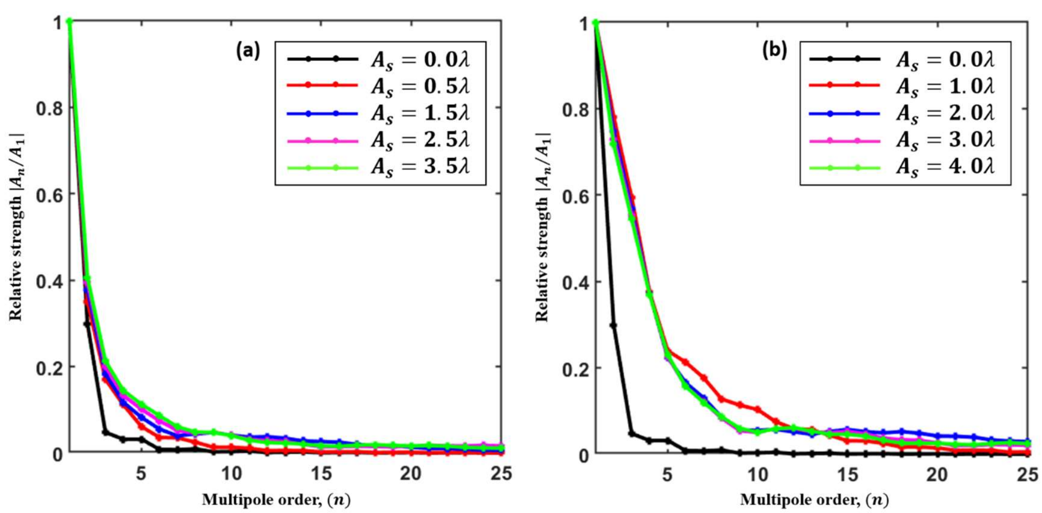

Fig. 5.11 Relative strength of the expansion coefficients for a tightly focused linearly polarized beam ($\alpha = 60°$) under a spherical aberration, $|A_n/A_1|$ for (a) half-integral coefficients, and (b) integral coefficients.

Variations of intensity enhancement with size of nanoparticles are presented in Fig. 5.12, and Fig. 5.13, and the step size on the horizontal axis are 10 nm. Results for an aberration free system, i.e. ($A_s = 0.0\lambda$) are also compared with results of system with a spherical aberrations $A_s = 1.0\lambda$. Figs. 5.12 (a), and (b) show the change in average radial and tangential intensity enhancement for the different radii of an Au nanoaprticle in the air whereas results in BK7 (glass) are presented in Figs. 5.12 (c), and (d). For an Au nanoparticle the incident wavelength is 550 nm.

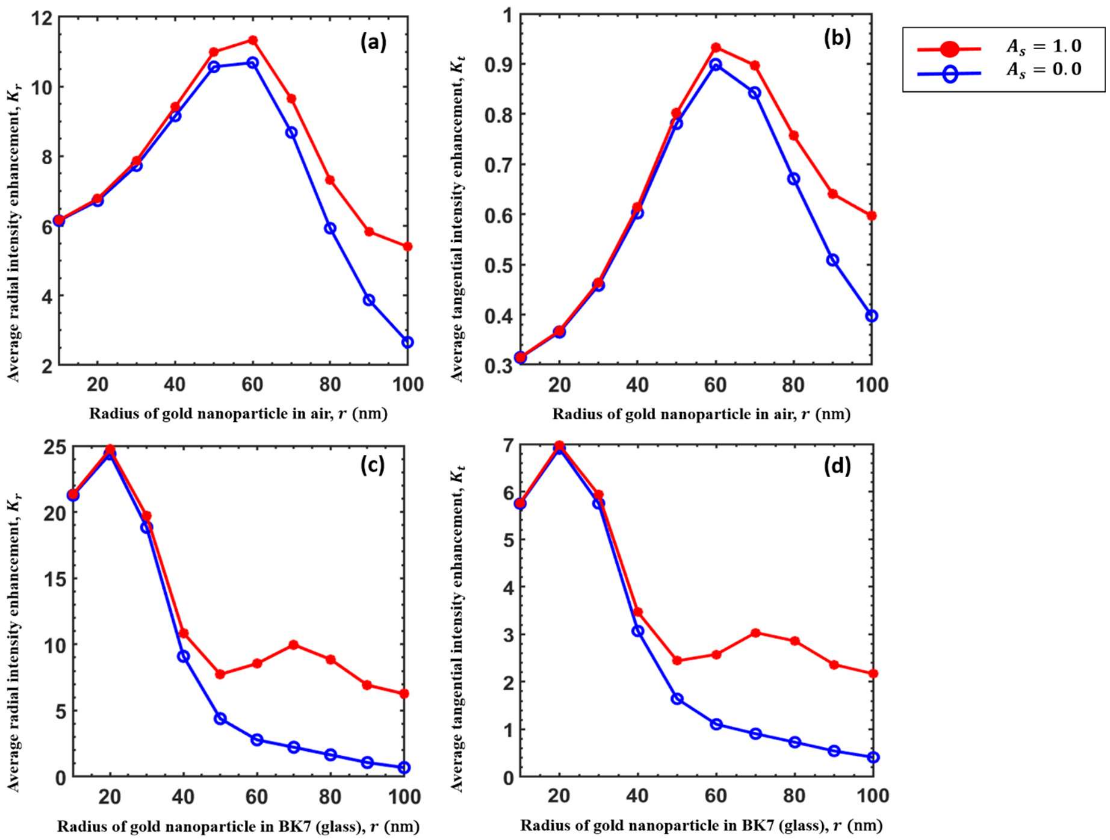

Fig. 5.12 Average radial and tangential intensity enhancement factor with varying radius of an Au nanoparticle in (a), (b) air, and (c), (d) BK7 (glass) respectively, for $\boldsymbol{A_s = 0.0\lambda}$ (without spherical aberration), and $\boldsymbol{A_s = 1.0\lambda}$ (with spherical aberration).

In case of an Ag nanoparticle, 440 nm wavelength of incident beam is considered, and the results are plotted in Fig. 5.13 (a-d). Figs. 5.13(a), and (b) includes the average radial and tangential intensity enhancement for varying radius of an Ag nanoparticle in air. The intensity enhancement factor for an Ag nanoparticle in BK7 (glass) medium and with different radius from 10 nm to 100 nm are shown in Figs. 5.13 (c), and (d).

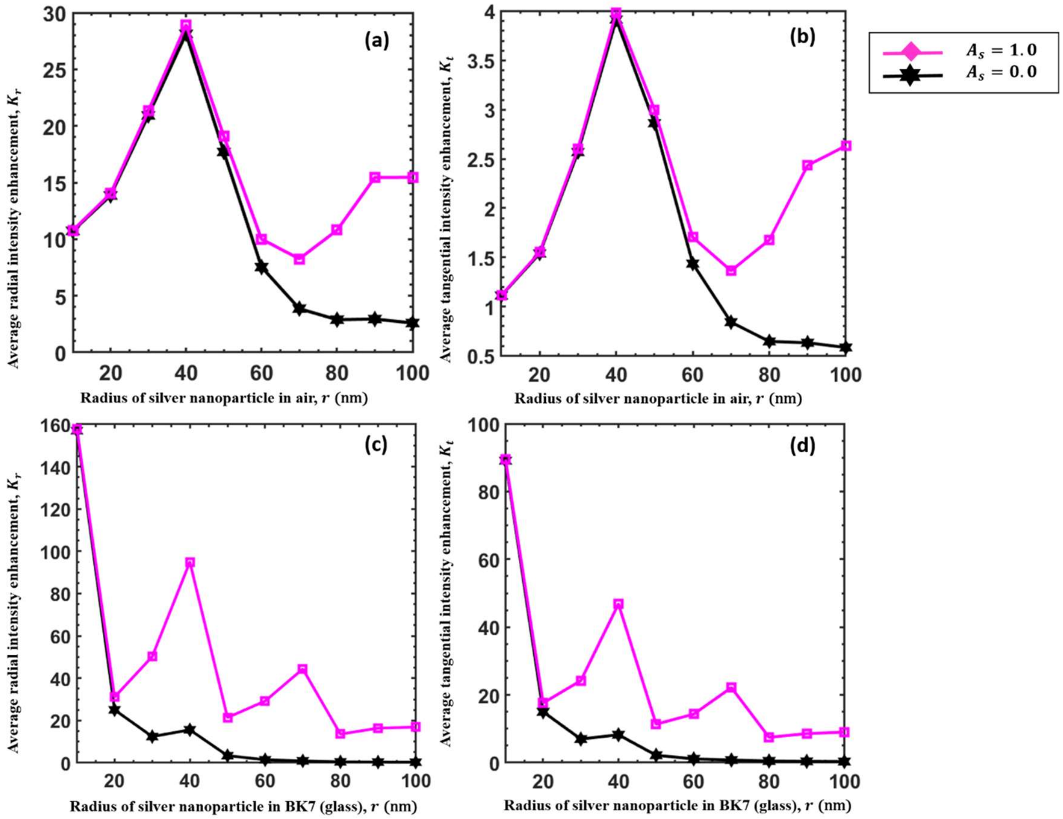

Fig. 5.13 Average radial and tangential intensity enhancement factor with varying radius of an Ag nanoparticle in (a), (b) air, and (c), (d) BK7 (glass) respectively, for $\boldsymbol{A_s = 0.0\lambda}$ (without spherical aberration), and $\boldsymbol{A_s = 1.0\lambda}$ (with spherical aberration).

Results in Fig. 5.12, and Fig. 5.13 show that the effect of spherical aberration is insignificant for a smaller size Au and Ag nanoparticle. On the contrary, enhancement factor decreases for bigger size nanoparticle. Figs. 5.12, and 5.13 highlight that an Au and Ag nanoparticle with 50 nm size is optimum in different dielectric media for the intensity enhancement.

Further, the effect of spherical aberration in the system are reduced with a proper combination of defocus and spherical aberration, i.e. $A_d = -A_s$, and results are presented in Figs. 5.14 and,

Fig. 5.15. Here, the spherical aberration is $A_s = 1.0\lambda$ for two situations, firstly when the system is without defocus ($A_d = 0.0\lambda$) and secondly for defocus aberration with the balancing condition ($A_d = -A_s$). The results are also compared with an aberration free case ($A_s = 0.0\lambda$).

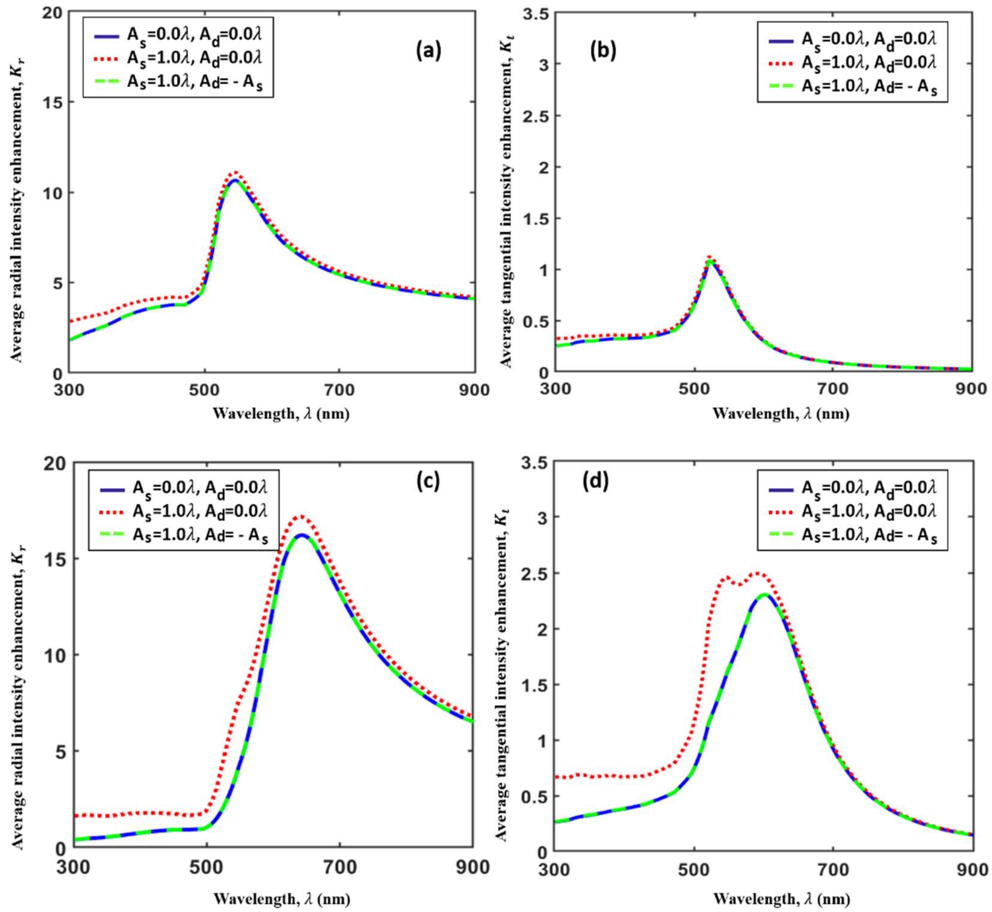

Fig. 5.14 Average radial and tangential intensity enhancement for an Au nanoparticle respectively, in (a), (b) air, and (c), (d) BK7 (glass) for a tightly focused linearly polarized beam with wavelength range 300 nm to 900 nm under three cases: (i) without aberration ($\boldsymbol{A_s = 0.0\lambda}$, $\boldsymbol{A_d = 0.0\lambda}$ (blue curve)) (ii) with spherical aberration ($\boldsymbol{A_s = 1.0\lambda, A_d = 0.0}$ (··· red curve)), and (iii) with spherical aberration and defocusing ($\boldsymbol{A_s = 1.0\lambda}$, $\boldsymbol{A_d = -A_s}$ (– – – green curve)).

The near-field intensity enhancement observed for an Au nanoparticle in air and BK7 (glass) medium is shown in Fig. 5.14. Figs. 5.14 (a), and (b) represent the average radial and tangential intensities respectively on the surface of an Au nanoparticle in air. The average radial and tangential intensity enhancements for an Au nanoparticle in glass are shown in Figs. 5.14 (c), and (d) respectively.

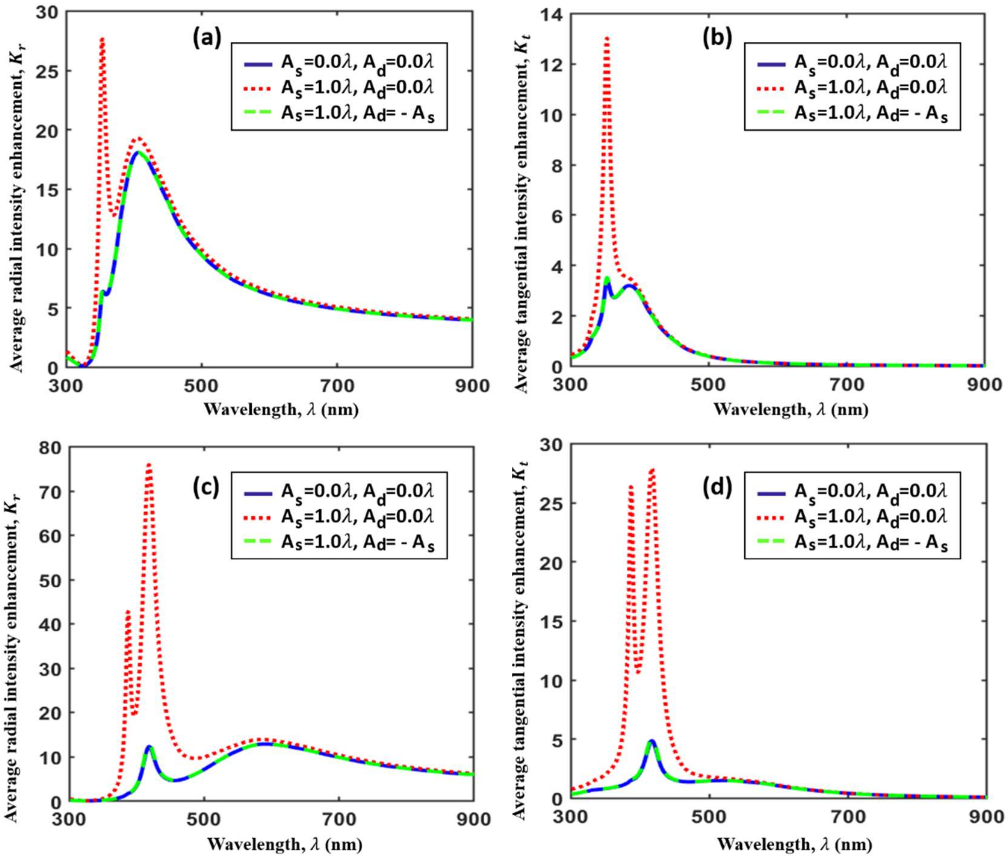

Fig. 5.15 Average radial and tangential intensity enhancement for an Ag nanoparticle respectively, in (a), (b) air, and (c), (d) BK7 (glass) for a tightly focused linearly polarized beam with wavelength range 300 nm to 900 nm and under three cases: (i) without aberration ($\boldsymbol{A_s = 0.0\lambda}$, $\boldsymbol{A_d = 0.0\lambda}$ (blue curve)) (ii) with spherical aberration ($\boldsymbol{A_s = 1.0\lambda, A_d = 0.0}$ (··· red curve)), and (iii) with spherical aberration and defocusing ($\boldsymbol{A_s = 1.0\lambda}$, $\boldsymbol{A_d = -A_s}$ (– – – green curve)).

The influence of defocus on the average radial and tangential intensity enhancement for an Ag nanoparticle in air is shown in Figs. 5.15 (a), and (b) respectively. For dielectric medium BK7 (glass), the respective near-field intensity enhancements are shown in Figs. 5.15 (c), and (d).

When the incident beam is aberration free i.e. $A_s = 0.0\lambda$, the maximum radial and tangential intensity enhancements are obtained at wavelengths 417 nm and 419 nm for an Ag nanoparticle of a radius 50 nm in the glass. From Figs. 5.6 to 5.9, it is observed that the maximum intensity enhancements are observed around 418nm wavelength for a spherically aberrated system. Further, an analysis is done to examine effect of NA on the near field enhancement at a fixed wavelength 418 nm. Fig. 5.16 presents the average radial and tangential intensity enhancements for a system with spherical aberration, and convergence angle range $\alpha = 5°$ to $\alpha = 90°$.

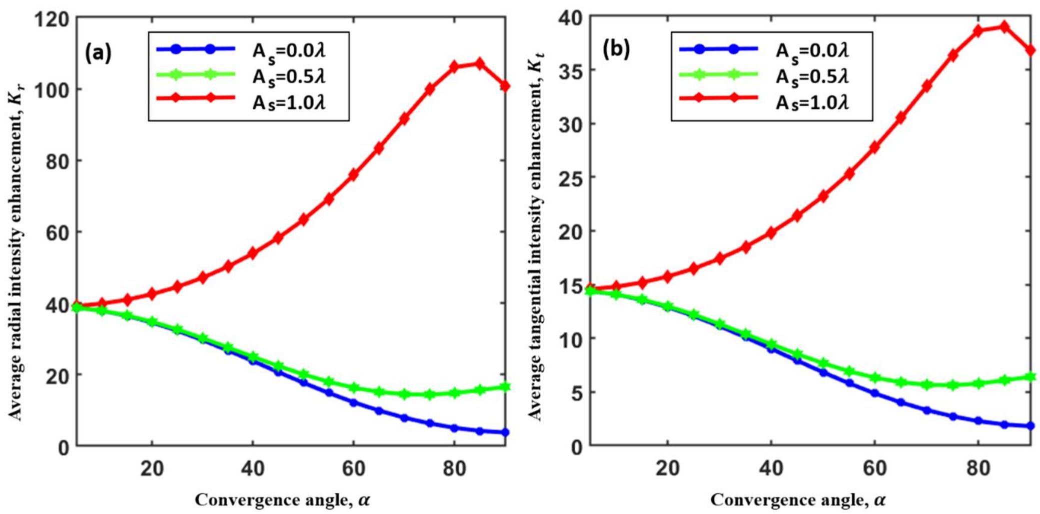

Fig. 5.16 For an Ag nanoparticle in BK7 (glass) medium the average (a) radial, and (b) tangential intensity enhancement varying with convergence angle for different values of spherical aberration $\boldsymbol{A_s}$, at wavelength 418 nm. $\boldsymbol{A_s = 0.0\lambda}$ (blue curve), $\boldsymbol{A_s = 0.5\lambda}$ (green curve) $\boldsymbol{A_s = 1.0\lambda}$ (red curve).

A significant enhancement in near-field intensities is observed for focusing of a beam with high convergence angle as shown in Fig. 5.16 (a), and (b) for $A_s = 1.0\lambda$ in comparison to $A_s = 0.5\lambda$. In contrast, focusing of beam with low convergence angle shows lesser increase in average radial and tangential intensity enhancements as shown in Fig. 12(a), and (b).

5.6 Conclusion

The plasmonic response of a spherically symmetric nanoparticle is theoretically analyzed using the Mie theory and multipole expansion for a tightly focused beam under the spherical aberration and defocusing. Mie scattering algorithm is developed by combining Richard and Wolf's formalism, and Zernike polynomials with Mie scattering for a tightly focused linearly polarized beam. A detailed numerical analysis is carried out on the MATLAB platform and numerical codes are developed for this purpose. The scattering is examined in two different dielectric media namely air, and BK7 (glass). The near-field intensity enhancement of a metallic nanoparticle is affected by scattering behaviour, and it is notably amplified in the presence of spherical aberration. An enhancement in the near-field intensity appears due to excitement of plasmons on the surface of a nanoparticle and this is further increased for a beam under spherical aberration. In contrast to the aberration free case where radial component was dominating in the near field intensity enhancement, presence of spherical aberration in the focusing system significantly enhances the contribution of the tangential component in addition to the radial component. The effects of spherical aberration are reduced by using a proper combination of coefficients of spherical aberration and defocusing. The effect of high NA aplanatic lens used for tightly focusing the beam is also analyzed by making a comparison with low NA system. In an aberrated system low-NA beams also show enhancement in comparison to system where aberration was not considered.